# Supporting Information

## Daniau et al. 10.1073/pnas.1214292110

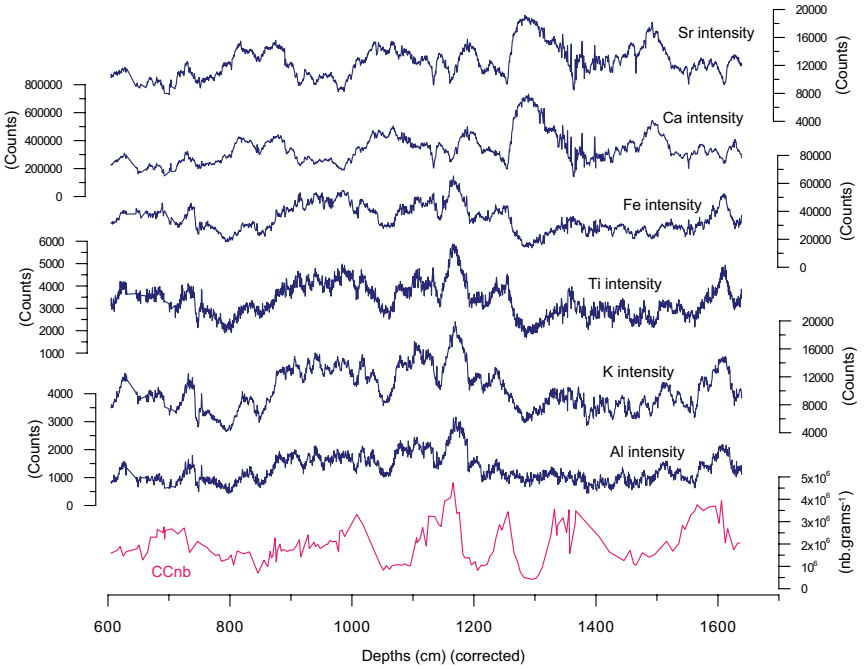


**Fig. S1.** Comparison between microcharcoal concentration expressed in number of particles per gram (CCnb) and X-ray fluorescence (XRF) core scanner data (intensity) against corrected depth from core MD96-2098.

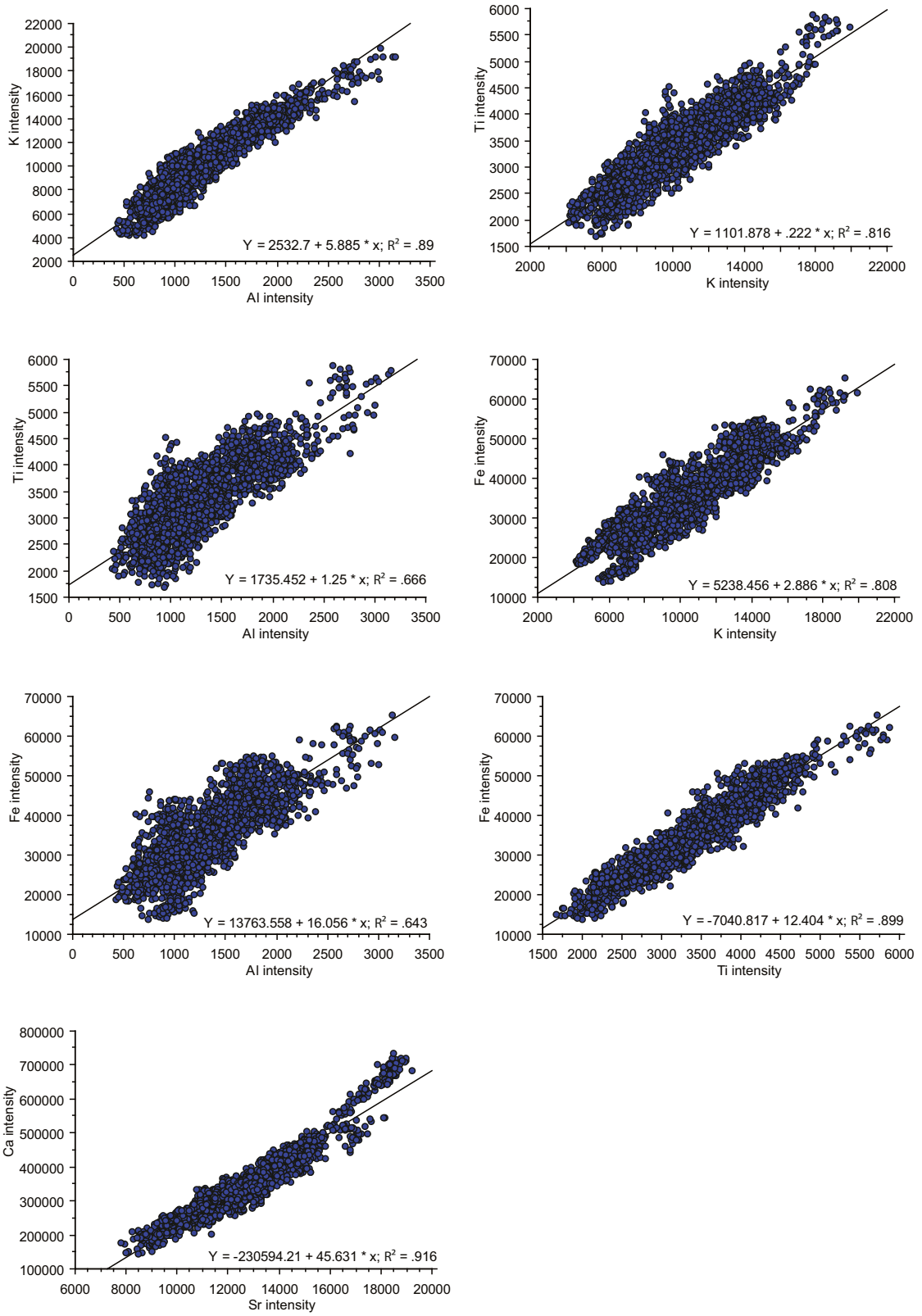


**Fig. S2.** Scatter plot of XRF core scanner data and associated correlation coefficient from core MD96-2098. Ca and Sr intensities showed a fairly strong positive linear correlation. We hence used Ca intensity to standardized microcharcoal concentration to the biogenic fraction. Al, K, Ti, and Fe intensity were positively correlated and are part of the terrigenous fraction. Al-K, K-Ti, K-Fe, and Ti-Fe showed a stronger correlation than Al-Ti and Al-Fe. We used therefore the sum of elements (Al+K+Ti+Fe) to standardized microcharcoal concentration to the terrigenous fraction.

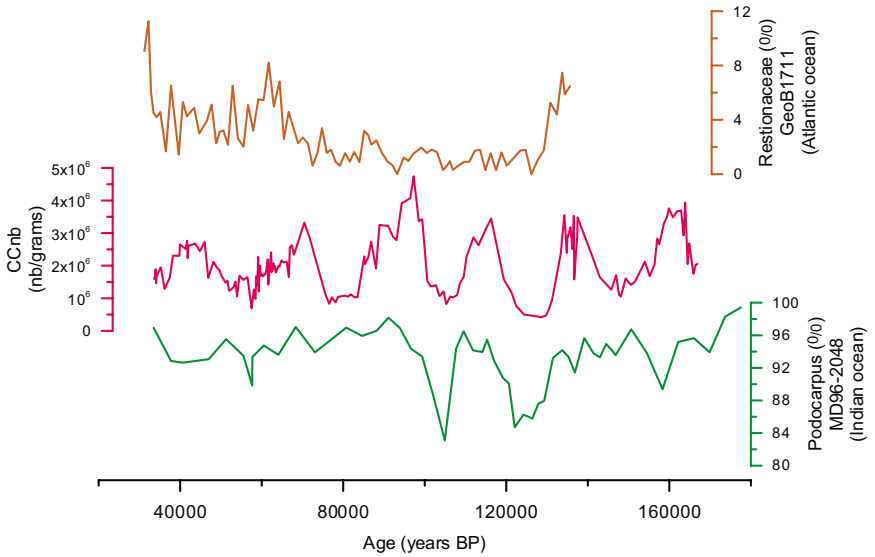


**Fig. S3.** Comparison between microcharcoal concentration expressed in number of particles per grams (CCnb, pink) and pollen percentages. (Bottom to top) Green curve represents *Podocarpus* pollen percentages of core MD96-2048 located in the Indian ocean (1), CCnb, brown curve corresponds to Restionaceae pollen percentages (fynbos) of core GeoB1711 located in the Atlantic ocean (1).

1. Dupont L (2011) Orbital scale vegetation change in Africa. *Quat Sci Rev* 30(25-26):3589–3602.

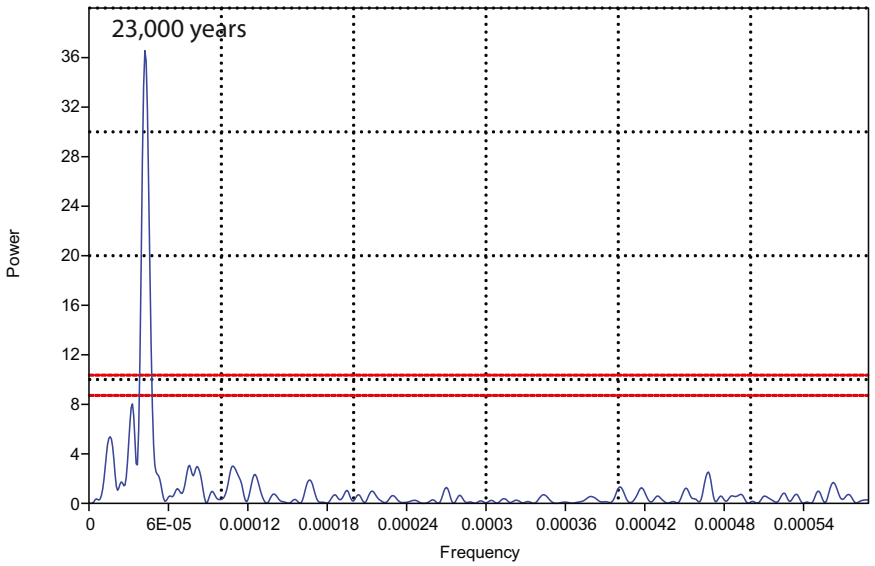


**Fig. S4.** Spectral analysis of microcharcoal concentration expressed in number of particles per gram (CCnb) using PAST software (1). The Lomb periodogram algorithm for unevenly sampled data was applied. The data were automatically detrended before the analysis. Red dashed lines indicate the 0.01 and 0.05 significance levels.

1. Hammer Ø, Harper DAT, Ryan PD (2001) PAST: Paleontological Statistics Software Package for Education and Data Analysis. *Palaeontologia Electronica* 4(1). Available at http://palaeo-electronica.org/2001_1/past/issue1_01.htm.

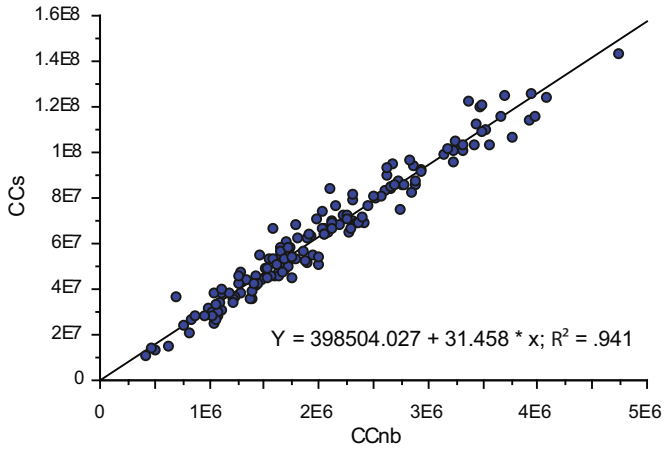


**Fig. S5.** Scatter plot between microcharcoal concentration expressed in number of particles per gram (CCnb) against microcharcoal concentration expressed in surface area per gram (CCs) from core MD96-2098. CCnb and CCs showed a strong positive linear relationships ($R^2 = 0.941$; $r = 0.97$, $P < 0.001$).

**Table S1. Chronostratigraphic age model for core MD96-2098**

| Laboratory code/event | Depth (cm) (uncorrected) | Depth (cm) (corrected)* | Material | AMS $^{14}$C y BP† | Error y (±) | 95.4% (2σ) cal y BP | Age (ka) | Ref(s). |
|---|---|---|---|---|---|---|---|---|
| SacA 24476 | 22.5 | — | *Neogloboquadrina pachyderma* (dextral) | 2,850 | 30 | 2,305–2,489 | 2.4 | |
| SacA 23251 | 65 | — | *N. pachyderma* (d) | 6,105 | 30 | 6,282–6,433 | 6.4 | |
| SacA 24477 | 150 | — | *N. pachyderma* (d) | 10,775 | 40 | 11,730–12,083 | 11.9 | |
| SacA 23252 | 241 | — | *N. pachyderma* (d) | 15,300 | 50 | 17,650–18,074 | 17.9 | |
| SacA 23253 | 331 | — | *N. pachyderma* (d) and *Globigerina bulloides* | 18,010 | 60 | 20,416–21,223 | 20.8 | |
| SacA 24478 | 481 | — | Bulk | 24,200 | 120 | 27,985–28,706 | 28.4 | |
| SacA 24479 | 561 | — | Bulk | 28,890 | 180 | 31,909–33,233 | 32.6 | |
| SacA 24480 | 647 | — | *N. pachyderma* (d) | 30,430 | 210 | 33,956–34,994 | 34.6 | |
| SacA 23254 | 719 | 704 | Bulk | 40,010 | 520 | 42,738–44,409 | 43.6 | |
| MIS 3.3 | 740 | 725 | | | | | 46 | 1 |
| MIS 4.0 | 1,000 | 837 | | | | | 57 | 1 |
| MIS 4.23 | 1,120 | 957 | | | | | 64 | 1 |
| MIS5/MIS4 | 1,195 | 1,032 | | | | | 73.5 | 2 |
| MIS 5.1 | 1,250 | 1,087 | | | | | 82 | 1 |
| MIS 5.2 | 1,280 | 1,117 | | | | | 87 | 1 |
| MIS 5.3 | 1,360 | 1,197 | | | | | 103.8 | 3 |
| MIS 5.4 | 1,400 | 1,237 | | | | | 110.4 | 3 |
| Onset MIS5 | 1,460 | 1,297 | | | | | 129 | 4 |
| MIS6/MIS5 | 1,500 | 1,337 | | | | | 135 | 5 |
| MIS 6.2 | 1,560 | 1,397 | | | | | 140 | 1 |
| MIS 6.4 | 1,730 | 1,567 | | | | | 160 | 1 |
| MIS 6.5 | 1,880 | 1,717 | | | | | 175 | 1 |
| MIS7/MIS6 | 2,000 | 1,837 | | | | | 191 | 1 |

*Apparent sediment gaps were reported on the stratigraphic log. Calculated corrected depths eliminate the apparent hiatus.
†We used a global reservoir age correction of 400 y, plus 157 y for local Δ R.

1. Lisiecki LE, Raymo ME (2005) A Pliocene-Pleistocene stack of 57 globally distributed benthic d18O records. *Paleoceanography* 20(1):1–17.
2. Sánchez-Goñi MF, Harrison SP (2010) Millennial-scale climate variability and vegetation changes during the last glacial: concepts and terminology. *Quat Sci Rev* 29:2957–2980.
3. Drysdale RN, et al. (2007) Stalagmite evidence for the precise timing of North Atlantic cold events during the early last glacial. *Geology* 35:77–80.
4. Masson-Delmotte V, et al. (2010) Abrupt change of Antarctic moisture origin at the end of Termination II. *Proc Natl Acad Sci USA* 107(27):12091–12094.
5. Henderson GM, Slowey NC (2000) Evidence from U-Th dating against Northern Hemisphere forcing of the penultimate deglaciation. *Nature* 404(6773):61–66.